

# Lipid and chitin nanofiber production during cultivation of the marine diatom *Cyclotella* sp. to high cell density with multistage addition of silicon and nitrate

Altan Ozkan<sup>1</sup> · Gregory L. Rorrer<sup>1</sup>

Received: 9 January 2017 / Revised and accepted: 2 March 2017 / Published online: 21 March 2017  
© Springer Science+Business Media Dordrecht 2017

**Abstract** The centric marine diatom *Cyclotella* sp. requires silicon in the form of  $\text{Si}(\text{OH})_4$  for cell wall biosynthesis, makes lipids for biofuels, and extrudes novel chitin nanofibers as a valued co-product for biomedical and nutraceutical applications. Due to the low solubility of  $\text{Si}(\text{OH})_4$  in seawater (<2 mM), to achieve high cell number density, dissolved Si was added in steps, with Si consumption between each step. A multistage nutrient delivery process with 19 mM cumulative Si delivery achieved a cell number density of  $4 \cdot 10^7$  cells  $\text{mL}^{-1}$  (5.0 g ash-free dry weight (AFDW)  $\text{L}^{-1}$ ), ten times higher than that of the two-stage Si addition process. Cell number and chitin production profiles were linear with time, commensurate with the Si consumption profile. The productivities of biomass and chitin were  $0.29$  g AFDW  $\text{L}^{-1} \text{ day}^{-1}$  and  $45$  mg chitin  $\text{L}^{-1} \text{ day}^{-1}$ , with chitin yield of 19 wt% in the biomass. Lipid production could not be sustained due to light attenuation, and yield decreased from 39 wt% (two-stage process) to 8 wt% (multistage process).

**Keywords** Chitin · Diatom · Lipid · Silicon · Nanofiber · Nutrient delivery

## Introduction

Diatoms are a clade of microalgae that possess intricately patterned porous cell walls of biosilica called frustules, and require dissolved silicon in the form of  $\text{Si}(\text{OH})_4$  for frustule

formation (Martin-Jézéquel et al. 2000). Diatoms are of considerable interest as a platform organism for algal biorefineries, given their high lipid yield and productivity under diverse environmental conditions (Hildebrand et al. 2012; Levitan et al. 2014).

Diatoms within genera *Cyclotella* and *Thalassiosira* produce biofuel lipids approaching 40 wt% in the biomass (d'Ippolito et al. 2015). In addition to biofuel lipids, a particularly unique bioproduct material known only to these diatom genera is chitin nanofibers. Chitin is a linear biopolymer of *N*-acetyl glucosamine. In these diatoms, chitin nanofibers are extruded from selected pores on the frustule as pure rigid rods approximately 50 nm in diameter (McLachlan et al. 1965; Herth and Zugenmaier 1977; Herth 1979; Herth and Barthlott 1979) in  $\beta$ -crystalline form (Ogawa et al. 2011). Pure chitin nanofibers have a wide variety of biomedical, functional food, and advanced material applications (Jayakumar et al. 2010; Habibi and Lucia 2012; Azuma et al. 2014; Ding et al. 2014). Diatom-derived chitin can also be hydrolyzed to the widely used nutraceutical glucosamine, and since the chitin nanofibers are extruded from the cell in pure form, the product is not contaminated with proteinaceous materials characteristic of shellfish-derived chitin (Rorrer et al. 2016).

In previous work, we described how silicon starvation was harnessed to stimulate the accumulation of lipids in the photosynthetic marine diatom *Cyclotella* (Jeffryes et al. 2013), as well as the production of chitin nanofibers (Rorrer et al. 2016). The requirement of dissolved silicon as a substrate for cell division and its unique role in the diatom cell division cycle (Huysman et al. 2014) provide an opportunity to develop bioprocessing strategies for the production of metabolites where silicon delivery controls the cell division rate and final cell number density in concert with other nutrient, light, and  $\text{CO}_2$  delivery processes that promote carbon accumulation within the cell.

✉ Gregory L. Rorrer  
gregory.rorrer@oregonstate.edu

<sup>1</sup> School of Chemical, Biological, and Environmental Engineering, Oregon State University, Corvallis, OR 97331, USA

New phototrophic cultivation strategies are needed to intensify the production rate and yield of the biofuel lipids and the valued chitin nanofiber co-product in the diatom *Cyclotella*. To achieve high cell density in diatom culture, one process limitation is providing soluble silicon in the form of monosilicic acid,  $\text{Si}(\text{OH})_4$ . The solubility of  $\text{Si}(\text{OH})_4$  in seawater is only 1.5–1.7 mM at 25 °C (Krauskopf 1956; Kato and Kitano 1968; Kamatani and Riley 1979). To accommodate this limitation, and to provide the Si and N needed for high cell number density, both soluble Si and nitrate (N) will be periodically dosed to the diatom cell suspension at 24- and 72-h intervals, respectively. The soluble Si will be consumed between dosing intervals to keep its concentration below the solubility limit. In this study, we compare a multistage Si + N nutrient addition process with a two-stage Si addition process for cultivation of the centric marine diatom *Cyclotella* sp. in a bubble-column photobioreactor under  $\text{CO}_2$  delivery-replete conditions. The multistage process is designed to increase the cell number density by a factor of ten over to the two-stage process, from  $4 \times 10^6$  to  $4 \times 10^7$  cells  $\text{mL}^{-1}$ . The phototrophic productivity of biomass, total lipid, and chitin to this high cell number density will be assessed and compared to their  $\text{CO}_2$  and nutrient consumption profiles.

We report that the multistage Si + N addition process resulted in the linear production of cells and chitin with time, with a final chitin concentration of nearly 700  $\text{mg L}^{-1}$ . However, this process did not stimulate lipid production. Details are provided below.

## Materials and methods

**Diatom cell culture** Cultures of marine centric diatom *Cyclotella* sp. were originally obtained from the UTEX Culture Collection of Algae (UTEX #1269). The cell line was cultivated in 100 mL of autoclaved Harrison's ASM artificial seawater medium (Berges et al. 2001) enriched with 0.50 mM  $\text{Na}_2\text{SiO}_3$ , 5.0 mM  $\text{NaNO}_3$ , and 0.25 mM  $\text{NaH}_2\text{PO}_4 \cdot \text{H}_2\text{O}$  in 500-mL foam-stoppered glass flasks. Cell suspension cultures were incubated at 22 °C under 100  $\mu\text{mol photons m}^{-2} \text{s}^{-1}$  incident light intensity on a 14-h/10-h light/dark cycle, and subcultured at 10% v/v every 21 days using sterile technique in a laminar-flow hood. To facilitate gas exchange and disperse the suspension, each flask was swirled for 10 s once per day.

**Photobioreactor design and operating conditions** *Cyclotella* diatom cell suspensions were cultivated in the bubble-column photobioreactor modified from a design described previously (Rorrer et al. 2016). The photobioreactor was equipped for controlled temperature, external illumination, aeration gas delivery with controlled  $\text{CO}_2$  composition, and online  $\text{CO}_2$  exhaust gas monitoring. The bioreactor vessel

was a Pyrex glass tube of 10.5 cm inner diameter, 69 cm length, and a working volume of 4.5 L. The cultivation temperature was 22 °C. External illumination was provided by twelve 50-W halogen lamps (MR16, Phillips, 2800 K), arranged around the perimeter and length of the vessel. The incident light intensity was determined by the average of photosynthetically active irradiation (PAR) measurements at 1.25-cm intervals along the inner circumference and working depth of the vessel. The illumination photoperiod was fixed at 14 h light/10 h dark.

House air and  $\text{CO}_2$  gas (99.9% purity) were metered and controlled separately by mass flow controllers then mixed fed to the bottom of the vessel through a stainless steel, 2- $\mu\text{m}$  mesh solvent inlet filter to provide fine bubble aeration. The inlet gas flow rate was fixed at 500  $\text{mL min}^{-1}$ . The exhaust aeration gas  $\text{CO}_2$  composition was continuously monitored by infrared analysis using a LI-COR LI-820  $\text{CO}_2$  analyzer. The outlet gas  $\text{CO}_2$  concentration vs. time profile was used to estimate the cumulative consumption of  $\text{CO}_2$  per unit volume of culture ( $X_C$ ,  $\text{mmol C L}^{-1}$ ) according to the material balance relationship

$$X_C(t) = X_{C,0} + \frac{v_o P}{RT} \int_0^t \frac{1}{V_L} (y_{\text{CO}_2, \text{in}} - y_{\text{CO}_2, \text{out}}) dt \quad (1)$$

where  $v_o$  is the volumetric gas flow rate ( $\text{L gas min}^{-1}$ ),  $P$  is total system pressure (1.0 atm),  $T$  is temperature (295 K),  $R$  is the ideal gas constant,  $V_L$  is the current liquid volume (L), and  $y_{\text{CO}_2, \text{in}}$  and  $y_{\text{CO}_2, \text{out}}$  are the inlet and outlet  $\text{CO}_2$  gas mole fractions, respectively. The medium was buffered with  $\text{NaHCO}_3$  to maintain the culture pH at the desired  $\text{CO}_2$  partial pressure ( $\text{pCO}_2$ ) in the aeration gas, using methods described previously (Rorrer 2015). The  $\text{CO}_2$  delivery rate ( $\text{CO}_2\text{-TR}$ ,  $\text{mmol CO}_2 \text{ L}^{-1} \text{ culture h}^{-1}$ ) was determined from the inlet gas flow rate and  $\text{CO}_2$  concentration.

**Nutrient delivery** Process input parameters for the two-stage and multistage nutrient addition processes are compared in Table 1. In all nutrient addition scenarios, a concentrated solution of sodium metasilicate ( $\text{Na}_2\text{SiO}_3$ ) in distilled  $\text{H}_2\text{O}$  was delivered in known volume to achieve the desired final dissolved Si concentration diluted in the culture volume. Once the concentrate was dissolved in seawater, it speciated to  $\text{Si}(\text{OH})_4$  at the cultivation pH of 8.3–8.5. In the two-stage process, the diatom cells were grown up to silicon starvation in stage I, and then in stage II, 1.2 mM additional dissolved Si was added to the silicon-starved cells to enable approximately three more doublings. To achieve high cell number density, given the low solubility of  $\text{Si}(\text{OH})_4$  in seawater-based medium ( $<2$  mM), it was necessary to add the dissolved Si in steps and then allow the culture to consume it. Therefore, in the multistage process, Si and nitrate (N) were periodically added to the cell suspension. Specifically, soluble Si was added in 24-h

**Table 1** Input nutrient delivery parameters for two-stage and multistage photobioreactor cultivation of the diatom *Cyclotella* sp.

Process parameter		Two-stage Si addition	Multistage Si + N addition
Incident light intensity, $I_o$	$\mu\text{mol photons m}^{-2} \text{ s}^{-1}$	220	520
Aeration gas flow rate, $v_g/V_L$	$\text{L gas L}^{-1} \text{ culture min}^{-1}$	0.11	0.11
Aeration gas $\text{CO}_2$ partial pressure, $p\text{CO}_2$	ppm	3000	15,000
$\text{CO}_2$ -TR	$\text{mmol CO}_2 \text{ L}^{-1} \text{ h}^{-1}$	0.80	4.2
Medium bicarbonate concentration	$\text{mmol L}^{-1}$	17	44
Initial Medium pH		8.3	8.0
Initial Si loading	$\text{mmol Si L}^{-1}$	0.3	1.5
Initial nitrate loading	$\text{mmol N L}^{-1}$	7.0	10.0
Initial phosphate loading	$\text{mmol P L}^{-1}$	0.35	0.50
Cumulative Si loading	$\text{mmol Si L}^{-1}$	1.5	19.0
Number of Si addition steps		2	11
Cumulative nitrate loading	$\text{mmol N L}^{-1}$	7.0	31
Number of nitrate addition steps		1	4
Cumulative phosphate loading	$\text{mmol P L}^{-1}$	0.35	1.55

intervals to reset the culture Si concentration to 1.5–2.0 mM, and nitrate (as  $\text{NaNO}_3$ ) was added in 72-h intervals to reset the culture nitrate concentration at 10 mM to avoid nitrogen starvation during silicon uptake. Phosphate (as  $\text{NaH}_2\text{PO}_4 \cdot \text{H}_2\text{O}$ ) was also added along with the nitrate at a 1:20 M ratio (0.5 mM). To achieve high cell number density, it was also necessary to increase the light intensity and  $\text{CO}_2$  transfer rate to provide for the increased photosynthetic carbon assimilation. However, no additional micronutrients were added after the initial nutrient loading. Nutrient consumption was determined by material balance based on the nutrient added and its measured concentration in the liquid culture.

**Analytical methods** Diatom cell suspension samples pulled from the photobioreactor were assayed for cell number density, dissolved silicon concentration, dissolved nitrate concentration, ash-free dry weight (AFDW), total lipid, and chitin composition as described previously (Rorrer et al. 2016), with key details provided below. Cell number density was determined by a Beckman Z2 Coulter Counter at a minimum threshold of 6  $\mu\text{m}$ . Dissolved nitrate and silicon concentrations in the culture medium were determined by spectrophotometric assay. For determination of biomass content, aliquots of the sampled cell suspension were centrifuged at  $2000 \times g$  for 10 min, and the pellet was washed twice with 0.6 M NaCl solution. The centrifuged pellet was dried at  $80^\circ\text{C}$  in air for 18 h. The ash-free biomass content was obtained by measuring the loss on ignition of the samples at  $550^\circ\text{C}$  for 10 h in a furnace. Total lipid in the cell mass was assayed spectrophotometrically following centrifugation of 50 mL cell suspension ( $1000 \times g \times 10 \text{ min}$ ), drying of the centrifuged pellet ( $80^\circ\text{C}$ , 24 h), and solvent extraction of the dried pellet with 5 mL of 2:1 (v/v) chloroform/methanol for 12 h at room temperature under continuous shaking. The chitin content in the

biomass was determined by acid hydrolysis of the pellet from a centrifuged ( $16,000 \times g$ , 15 min) and washed diatom cell suspension sample (10 mL) in 8 M HCl at  $90^\circ\text{C}$  for 3 h to convert chitin to glucosamine. Glucosamine was quantified by high-performance liquid chromatography (HPLC) of the NaOH-neutralized and filtered sample using a Dionex MA-1 strong anion-exchange column at  $30^\circ\text{C}$ ,  $0.4 \text{ mL min}^{-1}$  0.75 M NaOH isocratic mobile phase eluent, and pulsed amperometric mode detection of the column effluent with a Dionex ED-40 electrochemical detector. All values were reported as the average of triplicate assay measurements.

## Results

**Nutrient delivery and consumption profiles for the two-stage and multistage processes** The cumulative nutrient consumption vs. time profiles for the two-stage and multistage photobioreactor cultivation experiments are compared in Fig. 1. For the two-stage process, the cumulative Si delivery was 1.5 mM. All the Si delivered to the cell suspension at the initiation of stage II was consumed within 48 h, and no dissolved Si remained in the medium. However, nitrate consumption was not complete until 240 h after the second Si addition (Fig. 1a).

In the multistage process, the cumulative Si delivery was 19 mM. The cultivation was allowed to proceed for 120 h after the first addition of 1.5 mM Si. Then, Si was added ten more times in 24-h intervals up to 336 h (Fig. 1b). After each dose, the dissolved Si concentration rapidly decreased but did not go to zero. This strategy resulted in a linear silicon consumption vs. time profile. Concurrently, the nitrate consumption vs. time profile was also linear. The rates of Si and N

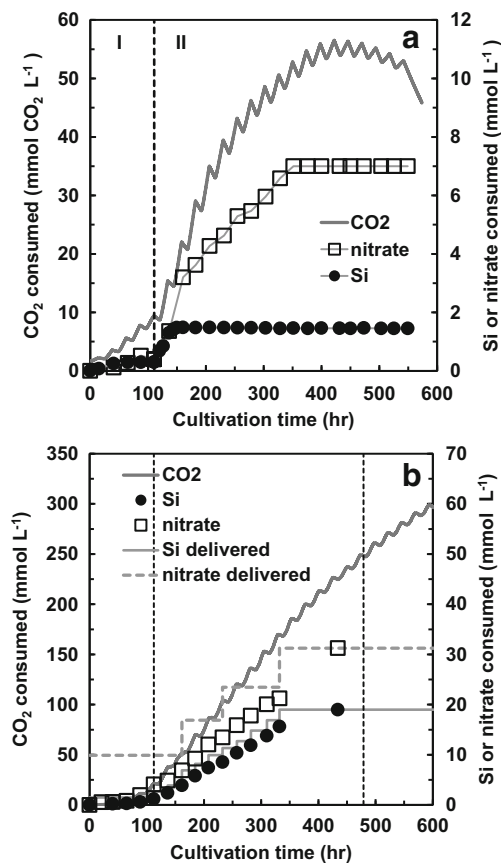


**Fig. 1** Comparison of the cumulative CO<sub>2</sub>, Si, and nitrate consumption profiles during photobioreactor cultivation of the diatom *Cyclotella* sp. **a** Two-stage Si addition; **b** multistage Si + N addition. The stepped lines indicate the Si and nitrate delivery profiles, the first vertical dotted line represents the transition to linear growth, and the second vertical dotted line indicates complete consumption of Si and N after the last incremental nutrient delivery

consumption, estimated from the least-squares fit of the Si and N vs. time data in the linear regime, are provided in Table 2.

The cumulative CO<sub>2</sub> consumption vs. time profiles shown in Fig. 1a (two-stage process) and Fig. 1b (multistage process) had a jagged shape, because during the dark phase of the photoperiod, CO<sub>2</sub> was released by respiration. Silicon and nitrate delivery had pronounced effects on the cumulative photosynthetic CO<sub>2</sub> consumption vs. time profile. In the two-stage cultivation experiments, CO<sub>2</sub> consumption continued after complete silicon consumption from the medium and did not level off until all of the nitrate was consumed. In the

**Table 2** Nutrient consumption rates, linear regime of the multistage photobioreactor cultivation process

Productivity parameter	Value and units	
Si consumption rate	0.059 ± 0.0025	mmol Si L <sup>-1</sup> h <sup>-1</sup>
Nitrate consumption rate	0.086 ± 0.0018	mmol N L <sup>-1</sup> h <sup>-1</sup>
CO <sub>2</sub> consumption rate	0.648 ± 0.0003	mmol CO <sub>2</sub> L <sup>-1</sup> h <sup>-1</sup>

All errors are 1.0 SE

multistage process, CO<sub>2</sub> consumption was nearly linear with time, commensurate with the Si and N consumption vs. time profiles. However, CO<sub>2</sub> consumption continued after complete consumption of Si and N from the medium, which would indicate that the intracellular storage of nutrients was sufficient to drive continued photosynthetic carbon assimilation. The cumulative amount of CO<sub>2</sub> consumed for the multistage process was about five to six times higher than that for the two-stage process.

**Biomass, lipid, and chitin productivity for the two-stage process** Cell biomass, total lipid, and chitin production vs. time profiles for photobioreactor cultivation of the diatom *Cyclotella* from the two-stage Si addition process are presented in Fig. 2. In stage II of the two-stage cultivation process, the biomass, lipid, and chitin concentration vs. time profiles were sigmoidal in shape. Lipid and chitin accumulated after silicon consumption from the medium, and formation of these products stopped at nitrate depletion. These data were fitted to the logistic model of the form:

$$C_{p-i} = \frac{C_{p-i,o} e^{k_{p-i} (t-t_0)}}{1 + \frac{C_{p-i,o}}{C_{p-i,f}} (e^{k_{p-i} (t-t_0)} - 1)} \quad (2)$$

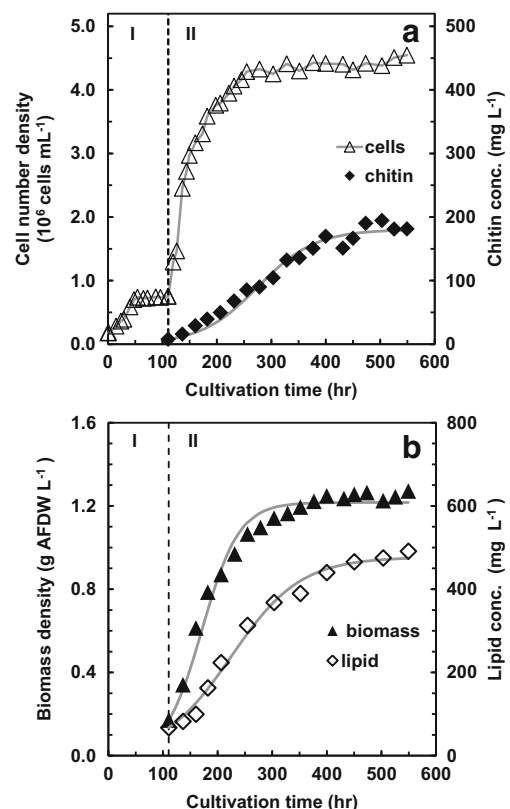


**Fig. 2** Cell biomass, total lipid, and chitin production for photobioreactor cultivation of the diatom *Cyclotella* with two-stage Si addition. **a** Cell number and chitin; **b** biomass and total lipid

In Eq. 2,  $C_{p-i}$  is the product concentration of  $i$ , where  $i$  represents cell number, biomass, lipid, or chitin (cells  $\text{mL}^{-1}$  or  $\text{mg L}^{-1}$ );  $C_{p-i,f}$  is the final product concentration (cells  $\text{mL}^{-1}$  or  $\text{mg L}^{-1}$ );  $k_{p-i}$  is the logistic model rate constant ( $\text{h}^{-1}$ );  $t$  is cultivation time in stage II (h); and  $t_o$  is the initial cultivation time in stage II ( $\text{h}^{-1}$ ). Estimates for fitted parameters  $C_{p-i,f}$  and  $k_{p-i}$  were obtained by non-linear, least-squares regression (NLS) using the Marquardt method (Statgraphics Centurion XVII software). Best-fit values for  $k_{p-i}$  were  $0.060 \pm 0.003$ ,  $0.036 \pm 0.002$ ,  $0.020 \pm 0.001$ , and  $0.019 \pm 0.001 \text{ h}^{-1}$  for cell number, biomass, lipid, and chitin, respectively (all errors 1.0 SE). Estimates for  $C_{p-i,f}$  are presented in Table 3.

The peak production rate ( $R_{p-i}$ ) was determined from the derivative of Eq. 2, given by

$$R_{p-i} = \left. \frac{dC_{p-i}}{dt} \right|_{\max} = \frac{k_{p-i}C_{p-i,f}}{4} \tag{3}$$

with total error estimated by propagation of the standard errors of the fitted parameters. Estimates of  $R_{p-i}$  for cell number, biomass, lipid, and chitin production for stage II of the two-stage process are provided in Table 3. Also provided in Table 3 are the final product yields of lipid (g lipid  $\text{g}^{-1}$  AFDW) and chitin (g chitin  $\text{g}^{-1}$  AFDW) in the biomass, which were determined by dividing the final concentrations of lipid and chitin to the final biomass concentration.

**Biomass, lipid, and chitin productivity for the multistage process** Cell biomass, total lipid, and chitin production vs. time profiles for photobioreactor cultivation of the diatom *Cyclotella* from the multistage Si + N addition process are presented in Fig. 3. Final cell number, biomass, lipid, and chitin yields for the multistage process are also presented in Table 3. The cell number vs. time profile of the multistage cultivation process was characterized by three regimes: an exponential phase at low cell number densities below  $4 \cdot 10^6$  cells  $\text{mL}^{-1}$ , a linear cell number vs. time phase under stepwise Si + N nutrient addition from  $4 \cdot 10^6$  to  $4 \cdot 10^7$  cells  $\text{mL}^{-1}$ , and a final resting phase following Si and nitrate depletion after cessation of Si + N delivery.

In the first 144 h of the linear phase at biomass densities below  $2.0 \text{ g AFDW L}^{-1}$ , the biomass and lipid concentration profiles were also linear with time (Fig. 3b). Least-squares estimates of the *initial* production rates for biomass and lipids in this linear range are presented in Table 3. However, above biomass densities of  $2.0 \text{ g AFDW L}^{-1}$ , both the biomass and lipid concentration profiles tapered off and became less than linear with time. At the end of nutrient Si + N delivery, both cell number and chitin production ceased at nitrate depletion. However, biomass production continued to increase past nitrate depletion, commensurate with its  $\text{CO}_2$  consumption vs. time profile.

The fraction of nitrogen incorporated into the chitin product relative to the cumulative nitrate delivered was comparable for the two-stage process (13% of fed nitrate to chitin-N) and the multistage process (11% of fed nitrate to chitin-N).

**Table 3** Comparison of productivity from two-stage and multistage photobioreactor cultivation of the diatom *Cyclotella* sp.

Process parameter	Variable and units	Two-stage Si addition	Multistage Si + N addition
<b>Volumetric production rates</b>			
	$R_{p-i}$		
Cell production rate	Cells $\text{mL}^{-1} \text{ day}^{-1}$	$1.4 \times 10^6 \pm 8 \times 10^4$	$2.8 \times 10^6 \pm 3 \times 10^4$
Biomass production rate	g AFDW $\text{L}^{-1} \text{ day}^{-1}$	$0.216 \pm 0.010$	$0.285 \pm 0.016$
Lipid production rate	mg lipid $\text{L}^{-1} \text{ day}^{-1}$	$45.1 \pm 2.2$	$30.1 \pm 2.9$
Chitin production rate	mg chitin $\text{L}^{-1} \text{ day}^{-1}$	$20.5 \pm 0.9$	$45.3 \pm 2.0$
<b>Final volumetric yields</b>			
	$C_{p-i,f}$		
Cell number density	Cells $\text{mL}^{-1}$	$4.3 \times 10^6 \pm 5 \times 10^4$	$4.4 \times 10^7 \pm 3 \times 10^6$
Biomass density	g AFDW $\text{L}^{-1}$	$1.2 \pm 0.02$	$5.0 \pm 0.1$
Lipid concentration	mg lipid $\text{L}^{-1}$	$477 \pm 10$	$369 \pm 27$
Chitin concentration	mg chitin $\text{L}^{-1}$	$180 \pm 5$	$691 \pm 49$
<b>Product yields in biomass</b>			
Lipid	g lipid $\text{g}^{-1}$ AFDW	$39.2\% \pm 0.9\%$	$8.1\% \pm 0.7\%$
Chitin	g chitin $\text{g}^{-1}$ AFDW	$14.8\% \pm 0.4\%$	$18.8\% \pm 0.2\%$
<b>Light transfer</b>			
Incident light intensity	$\mu\text{mol photons m}^{-2} \text{ s}^{-1}$	220	520
Light attenuation constant	$\text{mL } 10^6 \text{ cells}^{-1} \text{ cm}^{-1}$	$0.243 \pm 0.002$	$0.135 \pm 0.002$
Final mean light intensity	$\mu\text{mol photons m}^{-2} \text{ s}^{-1}$	82	34
% of $P_{o, \max}$		75%	44%

All errors are 1.0 SE



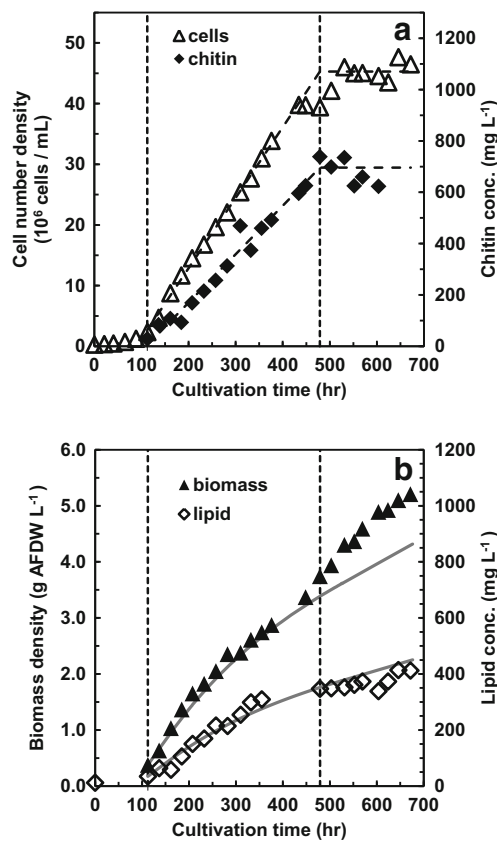


**Fig. 3** Cell biomass, total lipid, and chitin production for photobioreactor cultivation of the diatom *Cyclotella* with multistage Si + N addition. **a** Cell number and chitin; **b** biomass and total lipid. The first vertical dotted line represents the transition to linear growth, and the second vertical dotted line indicates complete consumption of Si and N after the last incremental nutrient delivery

However, the nitrate delivery at fixed Si delivery was not optimized in this study.

**Effects of light attenuation on biomass and lipid production from the multistage process** To quantify the effect of light attenuation on biomass and lipid productivity at high cell density in the multistage process, the mean light intensity ( $I_m$ ) for the photobioreactor cultivation process was estimated. For a cylindrical vessel with uniform external illumination,  $I_m$  is estimated from cell number density ( $X_N$ ) by

$$I_m(X_N) = \frac{4I_o e^{-k_c X_N R} \sinh(k_c X_N R)}{k_c X_N R} \quad (4)$$

where  $I_o$  is the average incident light intensity to the vessel surface ( $\mu\text{mol photons m}^{-2} \text{s}^{-1}$ ),  $R$  is the inner diameter of the vessel (cm), and  $k_c$  is the light attenuation constant for the culture ( $\text{mL cells}^{-1} \text{cm}^{-1}$ ). Light attenuation constants are provided in Table 3. The photosynthesis-irradiance curve of

*Cyclotella* diatom cells follows the exponential model of the form

$$\frac{P_o}{P_{o\max}} = 1 - e^{-I_m/I_k} \quad (5)$$

where  $I_k$  of  $59 \pm 2 \mu\text{mol photons m}^{-2} \text{s}^{-1}$  is the light intensity at 69.3% of photosynthetic saturation, based on previous photosynthetic oxygen evolution rate measurements (Rorrer et al. 2016). The relative photosynthetic oxygen evolution rate,  $P_o/P_{o\max}$ , represents the approach to light saturation. Calculated values for  $I_m$  and  $P_o/P_{o\max}$  at the end of the two-stage and multistage cultivation processes clearly show that high cell density reduced light transfer and decreased the relative photosynthetic rate (Table 3).

Based on consideration of Eqs. 4 and 5 above, for the multistage process, the biomass production rate under light attenuation is approximated by

$$\frac{dX}{dt} = r_{X,o} \cdot \left( 1 - e^{-I_m(X_N)/I_k} \right) \quad (6)$$

where  $r_{X,o}$  is the initial rate of biomass production ( $\text{g AFDW L}^{-1} \text{h}^{-1}$ ). Since the cell number density vs. time profile was linear during the entire nutrient delivery process, the cell production rate ( $r_N$ ,  $\text{cells mL}^{-1} \text{h}^{-1}$ ) is given by

$$\frac{dX_N}{dt} = r_N \quad (7)$$

Eqs. 6 and 7 were numerically integrated with time. The predicted biomass density vs. time curve under nutrient-replete conditions with light attenuation is shown by the solid line in Fig. 3b. A similar analysis was performed to generate the predicted lipid production vs. time curve, also shown in Fig. 3b. This simple analysis underpredicted biomass production but reasonably predicted lipid production. This result suggests that lipid production at high cell density decreased because of a reduction in photosynthetic rate resulting from light attenuation.

## Discussion

The centric marine diatom *Cyclotella* sp. makes lipids for biofuels and extrudes chitin nanofibers as a valued co-product. A simplified view of nutrient input and product formation within the centric marine diatom *Cyclotella* sp. is presented in Fig. 4. Key nutrient inputs are  $\text{CO}_2$  for cellular constituents and products,  $\text{Si(OH)}_4$  for biosilica cell wall biosynthesis and frustule formation, and nitrate ( $\text{NO}_3^-$ ) as the nitrogen (N) source for the *N*-acetyl glucosamine biopolymer (chitin) and other cellular constituents. The lipids are accumulated within the cell, whereas the chitin nanofibers are extruded from the

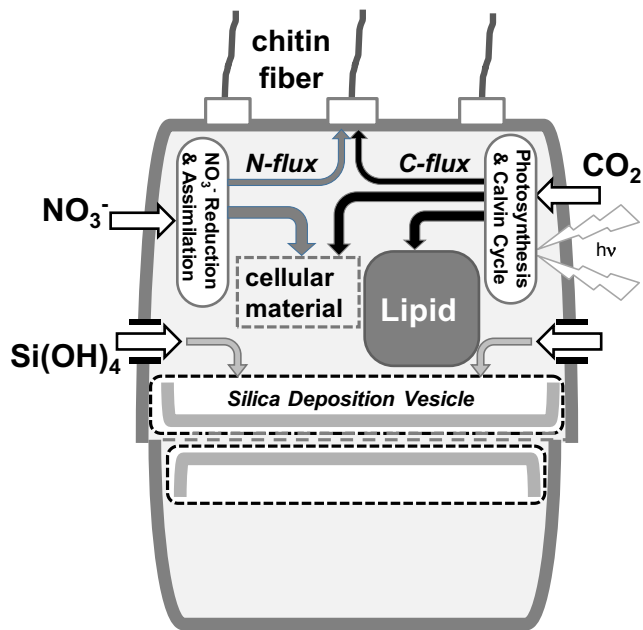


**Fig. 4** Highly simplified representation of key nutrient input and product formation in the diatom *Cyclotella*

cell through specialized pores called portulae lining the rim of the frustule. Although *Cyclotella* species are known to store  $\beta$ -1,3 glucan (chrysolaminarin) intracellularly, chitin is the only excreted polysaccharide (Gügi et al. 2015).

This study compared a two-stage Si addition process with a multistage Si + N nutrient addition process for cultivation of the centric marine diatom *Cyclotella* sp. in a bubble-column photobioreactor under  $\text{CO}_2$  delivery-replete conditions. The productivity of the two-stage process and that of the multistage process are compared in Table 3. Under a two-stage Si delivery process with 1.5 mM cumulative Si delivery, a final cell number density of  $4.3 \times 10^6$  cells  $\text{mL}^{-1}$  ( $1.2 \text{ g AFDW L}^{-1}$ ) was achieved and resulted in peak productivities of  $45 \text{ mg lipid L}^{-1} \text{ day}^{-1}$  and  $20 \text{ mg chitin L}^{-1} \text{ day}^{-1}$ , with  $39 \pm 0.9 \text{ wt\%}$  lipid and  $15 \pm 0.4 \text{ wt\%}$  chitin associated with the biomass. Both lipid and chitin production were stimulated after complete Si uptake. The lipid production rate exceeded the chitin production rate by at least a factor of two. The lipid and chitin profiles were sigmoidal in shape, commensurate with the Si and nitrate nutrient depletion profile.

In contrast, under a multistage Si + N nutrient delivery process with 19 mM cumulative Si delivery, the final cell number density was  $4.4 \times 10^7$  cells  $\text{mL}^{-1}$  ( $5.0 \text{ g AFDW L}^{-1}$ ), ten times higher than that of the two-stage process. The final cell number density was also commensurate with the cumulative amount of silicon delivered to the cell suspension. However, dissolved silicon had to be added in a series of ten stages because its solubility limit is approximately 2 mM. In the multistage process, the cell number and chitin production profiles were linear with time, consistent with the linear Si consumption vs. time profile, resulting in an initial lipid production rate

of  $30 \text{ mg L}^{-1} \text{ day}^{-1}$  and sustained chitin production rate of  $45 \text{ mg L}^{-1} \text{ day}^{-1}$ , with  $8.1 \pm 0.7 \text{ wt\%}$  lipid and  $19 \pm 0.2 \text{ wt\%}$  chitin and associated with the biomass.

The multistage process increased chitin productivity but decreased lipid productivity relative to the two-stage process. Furthermore, for the multistage process, the biomass and lipid concentration vs. time profile tapered off, whereas the cell number and chitin concentration vs. time profile remained linear. Both observations suggest that silicon delivery controlled cell division and chitin production, whereas photosynthetic carbon assimilation more strongly controlled biomass and lipid production per cell. The strong linear relationship between silicon consumption, cell number formation, and chitin production supports this conclusion.

While diatoms are unusually efficient at maintaining the cell division rate at low light efficiency (Nelson et al. 1979), this may not be true for photosynthetic carbon accumulation within the cell. The energetics of lipid vs. carbohydrate metabolism have not been characterized in diatoms. However, in green algae, lipid biosynthesis has a higher metabolic energy requirement than carbohydrate biosynthesis (Chen et al. 2013; Subramanian et al. 2013). It is suggested that light attenuation at high cell density lowered the mean light intensity experienced by the culture suspension at high cell density, and hence lowered the photosynthetic carbon accumulation rate per cell. Consequently, light attenuation could reduce the production of lipids more than chitin, which is a carbohydrate biopolymer. This process may also explain why the biomass carbon and lipid production tapered off over time, while cell number and chitin production remained constant with time.

In summary, based on this study, the multistage Si + N nutrient addition strategy enabled selective production of chitin over lipids at high cell density, because cell number and chitin production were determined by silicon delivery, whereas photosynthetic lipid production was promoted by light delivery, which could not be sustained due to light attenuation effects at high cell number density.

## Conclusions

The centric marine diatom *Cyclotella* sp. requires silicon in the form of  $\text{Si(OH)}_4$  for cell wall biosynthesis, makes lipids for biofuels, and extrudes chitin nanofibers as a valued co-product. Due to the low solubility of  $\text{Si(OH)}_4$  in seawater ( $<2 \text{ mM}$ ), a multistage Si + nitrate nutrient delivery process with 19 mM cumulative Si delivery was developed to achieve a cell number density of  $4 \times 10^7$  cells  $\text{mL}^{-1}$  ( $5.0 \text{ g AFDW L}^{-1}$ ), ten times higher than that of a two-stage Si addition process. Cell number and chitin production profiles were linear with time, commensurate with the Si consumption profile, with productivities of  $0.29 \text{ g AFDW L}^{-1} \text{ day}^{-1}$  biomass,  $45 \text{ mg L}^{-1} \text{ day}^{-1}$  chitin, and chitin yield in biomass of 19 wt%. Lipid production could

not be sustained due to light attenuation, and the yield decreased from 39 wt% (two-stage process) to 8 wt% (multistage process). Therefore, if the chitin nanofiber co-product is the target metabolite, then the multistage nutrient delivery process is recommended.

**Acknowledgements** This work was supported by the US National Science Foundation (NSF), Emerging Frontiers for Research and Innovation (EFRI) program, under award number 1240488.

## References

- d'Ippolito G, Sardo A, Paris D, Vella FM, Adelfi MG, Botte P, Gallo C, Fontana A (2015) Potential of lipid metabolism in marine diatoms for biofuel production. *Biotechnol Biofuels* 8:28
- Azuma K, Ifuku S, Osaki T, Okamoto Y, Minami S (2014) Preparation and biomedical applications of chitin and chitosan nanofibers. *J Biomed Nanotechnol* 10:2891–2920
- Berges JA, Franklin DJ, Harrison PJ (2001) Evolution of an artificial seawater medium: improvements in enriched seawater, artificial water over the last two decades. *J Phycol* 37:1138–1145
- Chen CY, Zhao XQ, Yen HW, Ho SH, Cheng CL, Lee DJ, Bai FW, Chang JS (2013) Microalgae-based carbohydrates for biofuel production. *Biochem Eng J* 78:1–10
- Ding F, Deng H, Du Y, Shi X, Wang Q (2014) Emerging chitin and chitosan nanofibrous materials for biomedical applications. *Nano* 6:9477–9493
- Gügi B, Costaouec TL, Burel C, Lerouge P, Helbert W, Bardor M (2015) Diatom-specific oligosaccharide and polysaccharide structures help to unravel biosynthetic capabilities in diatoms. *Mar Drugs* 13:5993–6018
- Habibi Y, Lucia LA (2012) Chitin nanofibers as building blocks for advanced materials. In: Habibi Y, Lucia LA (eds) *Polysaccharide building blocks: a sustainable approach to the development of renewable biomaterials*. John Wiley & Sons, NY, pp 227–245
- Herth W (1979) The site of  $\beta$ -chitin fibril formation in centric diatoms II. The chitin-forming cytoplasmic structures. *J Ultrastruct Res* 68:16–27
- Herth W, Barthlott W (1979) The site of  $\beta$ -chitin fibril formation in centric diatoms I. Pores and fibril formation. *J Ultrastruct Res* 68:6–15
- Herth W, Zugenmaier P (1977) Ultrastructure of the chitin fibrils of the centric diatom *Cyclotella cryptica*. *J Ultrastruct Res* 61:230–239
- Hildebrand M, Davis AK, Smith SR, Traller JC, Abbriano R (2012) The place of diatoms in the biofuel industry. *Biofuels* 3:221–240
- Huysman MJJ, Vyverman W, De Veylder L (2014) Molecular regulation of the diatom cell cycle. *J Exp Bot* 65:2573–2584
- Jayakumar R, Prabakaran M, Nair SV, Tamura H (2010) Novel chitin and chitosan nanofibers in biomedical applications. *Biotechnol Adv* 28:142–150
- Jeffryes C, Rosenberger J, Rorrer GL (2013) Fed-batch cultivation and bioprocess modeling of *Cyclotella* sp for enhanced fatty acid production by controlled silicon limitation. *Algal Res* 2:16–27
- Kamatani A, Riley JP (1979) Rate of dissolution of diatom silica walls in seawater. *Mar Biol* 55:29–35
- Kato K, Kitano Y (1968) Solubility and dissolution rate of amorphous silica in distilled and sea water at 20 °C. *J Oceanogr Soc Jpn* 24:147–152
- Krauskopf KB (1956) Dissolution and precipitation of silica at low temperatures. *Geochim Cosmochim Acta* 10:1–26
- Levitan O, Dinamarca J, Hochman G, Falkowski PG (2014) Diatoms: a fossil fuel of the future. *Trends Biotechnol* 32:117–124
- Martin-Jézéquel V, Hildebrand M, Brzezinski MA (2000) Silicon metabolism in diatoms: implications for growth. *J Phycol* 36:821–840
- McLachlan J, McInnes AG, Falk M (1965) Studies on the chitin (chitin: poly-N-acetylglucosamine) fibers of the diatom *Thalassiosira fluviatilis* Hustedt. I Production and isolation of chitin fibers. *Can J Bot* 43:707–712
- Nelson DM, D'Elia CF, Guillard RRL (1979) Growth and competition of the marine diatoms *Phaeodactylum tricornutum* and *Thalassiosira pseudonana*. II Light limitation. *Mar Biol* 50:313–318
- Ogawa Y, Kimura S, Wada M (2011) Electron diffraction and high-resolution imaging on highly-crystalline  $\beta$ -chitin microfibril. *J Struct Biol* 176:83–90
- Rorrer GL (2015) Bioprocess engineering of phototrophic marine organisms. In: Kim SK (ed) *Springer Handbook of Marine Biotechnology*. Springer, Heidelberg, pp 257–294
- Rorrer GL, Torres JA, Durst R, Kelly C, Gale D, Maddux B, Ozkan A (2016) The potential of a diatom-based photosynthetic biorefinery for biofuels and valued co-products. *Curr Biotechnol* 5:237–248
- Subramanian S, Barry AN, Pieris S, Sayre RT (2013) Comparative energetics and kinetics of autotrophic lipid and starch metabolism in chlorophytic microalgae: implications for biomass and biofuel production. *Biotechnol Biofuels* 6:1